Supporting Information

An In-depth Insight of Highly Reversible and Dendrite-Free Zn Metal Anode in Hybrid Electrolyte

Yuanjun Zhang,[a] *Ming Zhu,*[b] *Kuan, Wu,*[a] *Fangfang Yu,*[b] *Guanyao Wang,*[a] *Gang Xu,*[c,d] *Minghong Wu,**[c,d] *Hua-Kun Liu,*[b] *Shi-Xue Dou,*[b] *and Chao Wu**[a,b]

[a]School of Environmental and Chemical Engineering, Shanghai University, Shanghai 200444, China
[b]Institute for Superconducting & Electronic Materials, Australian Institute of Innovative Materials, University of Wollongong, NSW 2522, Australia
chaowu@uow.edu.au
[c]Shanghai Applied Radiation Institute, Shanghai University, Shanghai 200444, China
[d]Key Laboratory of Organic Compound Pollution Control Engineering (MOE), Shanghai University, Shanghai 200444, PR China
mhwu@shu.edu.cn

Experimental section

Materials

$ZnSO_4 \cdot 7H_2O$ and Glycerol were purchased from Adamas (Tansoole, China). Zn foil (50 μm and 9 μm in thickness) and stainless steel (SS) foil (9 μm in thickness) were purchased from Canrd (China).

Preparation of aqueous and hybrid electrolytes

A certain amount of $ZnSO_4 \cdot 7H_2O$ was dissolved into the deionized water to achieve 2 M ZnSO4 aqueous electrolyte. A certain amount of $ZnSO_4 \cdot 7H_2O$ was the mixed solution of deionized water and glycerol to prepare 2 M $ZnSO_4$ hybrid electrolytes with different content of glycerol.

Synthesis of $CaV_6O_{16} \cdot 3H_2O$ cathodes materials

$CaV_6O_{16} \cdot 3H_2O$ (CaVO) was synthesized via a conventional hydrothermal route according previous study[1].

Electrochemical measurements

The cyclic voltammetry (CV), linear scan voltammetry (LSV), chromoamperograms (CAs) and corrosion test were conducted on an electrochemical workstation (Autolab). The electrochemical

stability window was investigated in a three electrodes configuration, where the SS foil served as working, Pt served as the counter electrode, saturated calomel electrode (SCE) served as the reference electrode. In the corrosion test, the Zn foil was used as the working and counter electrodes and SCE was used as the reference electrode. The corrosion potential and corrosion current were calculated from Tafel fit system in electrochemical workstation. CA measurement used the Zn foil as working, counter, and reference electrodes. Electrochemical impedance spectroscopy (EIS) spectra were recorded on the electrochemical workstation with a frequency range from 0.1 MHz to 0.01 Hz.

Ionic conductivities were tested by two blocking electrodes (SS) and calculated according to the following equation:

$$\sigma = \frac{l}{R_b \cdot S}$$ Equation (S1)

CR2032 coin cells were used to evaluate the electrochemical behaviors of Zn plating/stripping. For the testing of Coulombic efficiency, the working electrode was the SS or Cu foil and the Zn foil served as the counter electrode, and a disk-like glass fiber paper worked as the separator. For the testing of symmetric cells, the disk-like Zn foils were used as the electrodes. The electrochemical performance of all samples was carried out by the LANHE battery tester (CT2001A, Wuhan LAND electronics Co., Ltd., China) at room temperature.

Material characterizations

The crystal structures of as-prepared samples were recorded by X-ray diffraction (XRD, Rigaku D/MAX2200V PC). The morphologies of as-prepared samples were investigated by scanning electron microscopy (SEM, Hitach S4800). H_2 gas was detection by gas chromatography (Shimadzu). Surface-based group analysis was conducted by X-ray photoelectron spectroscopy (XPS, Thermo Fisher Nexsa). *In-situ* optical microscopy (Zeiss Smartzoom 5) observation was carried out applying a special device provided by Beijing Science Star technology Co. Ltd.

Computational details

The structures of Zn^{2+}, SO_4^{2-}, H_2O, Glycerol and their complexes（Zn^{2+} with SO_4^{2-}, H_2O or Glycerol） were first optimized by using the density functional theory (DFT) at the ωB97XD/6-311G (d,p) level[2] in vacuum. In the meantime, all geometry optimizations including the implicit solvent effect with

SMD[3] were performed using the Gaussian 09 package.[4] Then the single-point energies of 3 complexes were done at the same level after previous optimization in a gas phase and in water respectively, which considering basis set superposition error (BSSE). The harmonic frequency calculations were carried out at the same level of theory to help verify that all structures have no imaginary frequency. Meanwhile, the Ghelp charge analysis of the optimized structures was carried out. Subsequently, these charged stable structures are applied to dynamics simulation through the Forcite module.

In order to further investigate the difference of adsorption of H_2O and glycerol on Zn electrode. Adsorption structures of them on Zn (101) surface were performed using the DMol3 program package in Materials Studio. The exchange and correlation terms were determined using the Generalized Gradient Approximation (GGA) in the form proposed by Perdew, Burke, and Ernzerhof (PBE).[5] Solvation effects were incorparated by COSMO solvation model for all the systems with water as solvent.

The interaction energy of 3 possible interaction patterns of the molecules (Einter) was calculated by the following equation:

$$E_{\text{inter}} = E_{AB} - (E_A + E_B) + E_{\_BSSE} \qquad \text{Equation (S2)}$$

Where E_A and E_B respectively represent the energies of A (Zn^{2+}) and B (SO_4^{2-}, H_2O or Glycerol) ,the $E_{\_BSSE}$ is the BSSE corrected energy of each interaction patterns and the E_{inter} is the total energy of one of 3 possible interaction patterns , a negative value of Einter indicates that the process is an exothermic reaction and high negative value corresponds to a stronger interaction, which indicates more heat release and a more stable product.

Two MD simulation models containing Zn^{2+}, SO_4^{2-} and aqueous solution were built with or without glycerol molecules. The initial numbers of each component are H_2O:$ZnSO_4$=1000:36 for 2 m $ZnSO_4$ aqueous electrolyte, and H_2O:$ZnSO_4$:glycerol= 1000:72:200 for 2 m $ZnSO_4$ in water/glycerol (50/50) electrolyte, which is in strict agreement with our experimental data. After energy minimization to remove potential overlaps among all molecules, 3 ns simulations of this system were performed in order to obtain an equilibrium state at constant temperature and pressure (NPT) with periodic boundary cell optimized. Finally the initial system was built in a cube simulation box, of which the dimensions was x = 41.6 Å, y = 41.6 Å, and z = 41.6 Å, respectively. During the simulation, periodic boundary conditions were applied in all three dimensions.

The MD simulation of different systems can be performed after charges and potentials are assigned

to each atom. The long-range electrostatic interactions have been accounted for using the Ewald method. The total energy is written as a combination of valence terms including diagonal and off-diagonal cross-coupling terms and nonbond interaction terms, which include the Coulombic and Lennard-Jones functions for electrostatic and van der Waals interactions,[6]

$$E = E_{\text{bonds}} + E_{\text{angles}} + E_{\text{dihedrals}} + E_{\text{cross}} + E_{\text{VDW}} + E_{\text{elec}} \qquad \text{Equation (S3)}$$

where E_{VDW} and E_{elec} are given by the eq 4:

$$E_{\text{non-bond}} = E_{\text{VDW}} + E_{\text{elec}} = \sum \varepsilon_{ij} \left[2\left(\frac{\sigma_{ij}}{r_{ij}} \right)^{9} - 3\left(\frac{\sigma_{ij}}{r_{ij}} \right)^{6} \right] + \sum \frac{q_i q_j}{r_{ij}} \qquad \text{Equation (S4)}$$

The parameters for each like-site interaction are given by the COMPASS force field. [7-8] The energies of the initial configurations are minimized with the Smart Minimizer method. After the minimization, all simulations are equilibrated at constant temperature and volume (NVT) for about 20 ns. Atomic coordinates were saved for every 500 ps. The analysis was performed by averaging over the final 1ns of each trajectory.

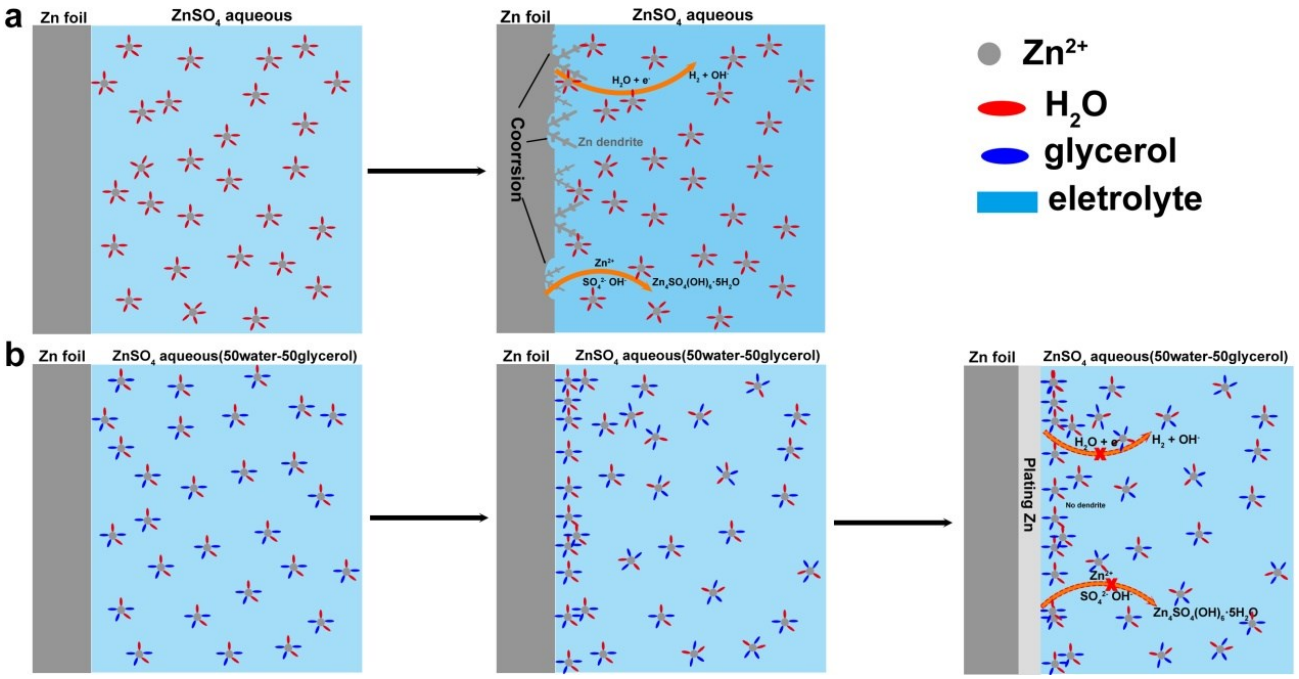

Figure S1. Schematic illustrations of Zn deposition (a) 2 M $ZnSO_4$ aqueous electrolyte or (b) 2 M $ZnSO_4$ glycerol/water (50/50) electrolyte.

Figure S2. Digital photos of the working electrode, the counter electrode, and the separator (Post-mortem cell after short-circuit)

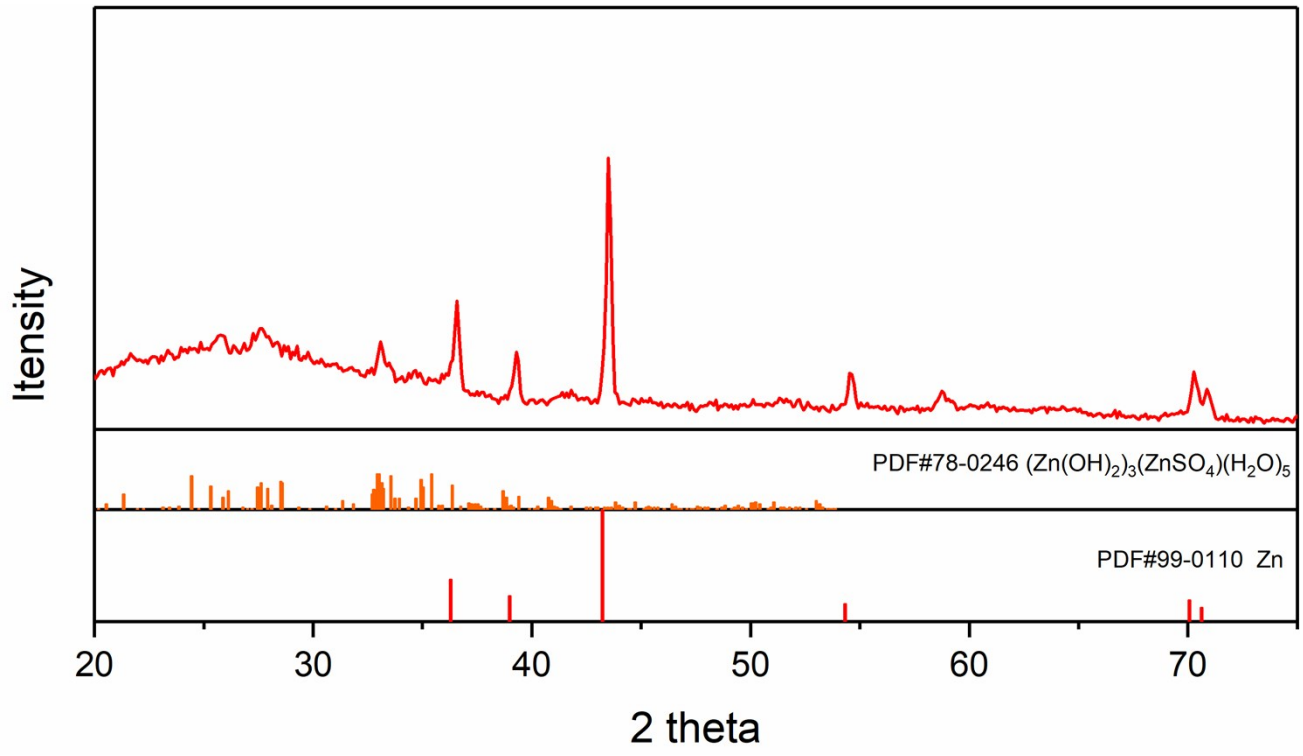

Figure S3. XRD pattern of the dendrites adhered to the glass fiber.

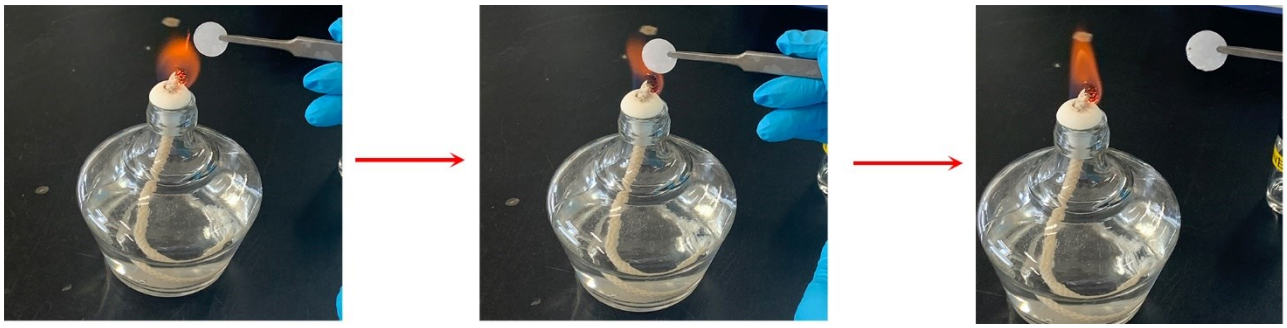

Figure S4. Photographs of the ignition tests of the glass fibers saturated with glycerol/water (50/50) hybrid electrolyte.

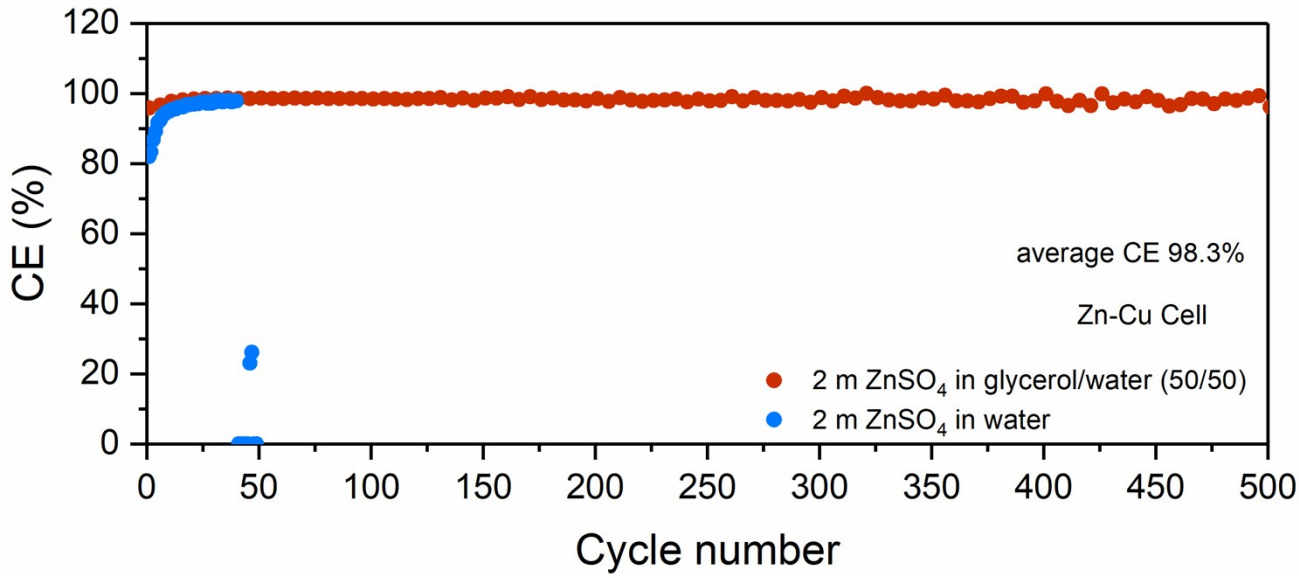

Figure S5. Coulombic efficiency of Zn plating/stripping cycles on the Cu substrate at 1 mA cm^{-2} and 1 mAh cm^{-2}.

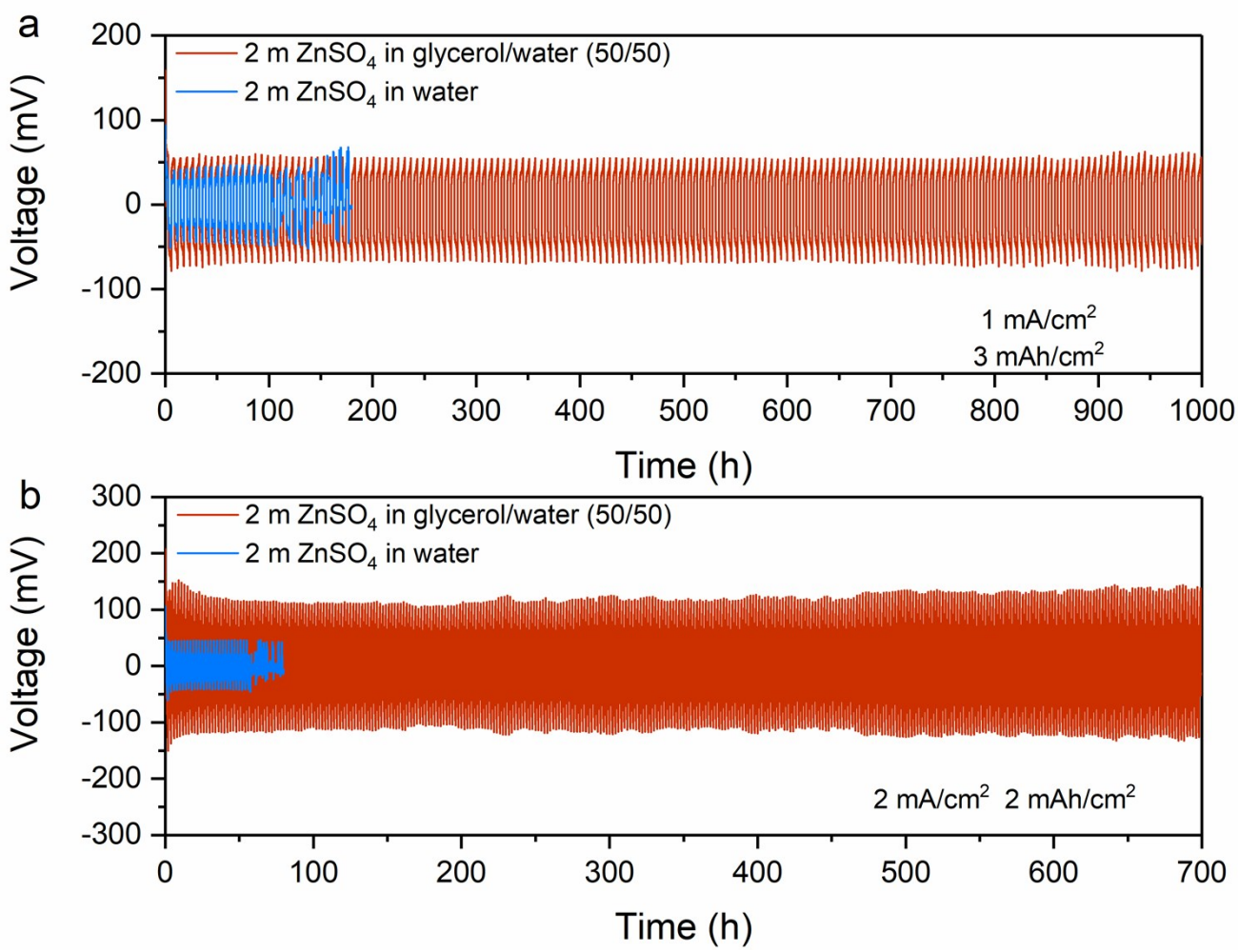

Figure S6. Voltage profiles of symmetric cells as a function of time at (a) 3 mAh cm^{-2} and 1 mA cm^{-2}, (b) 2 mAh cm^{-2} and 2 mA cm^{-2}

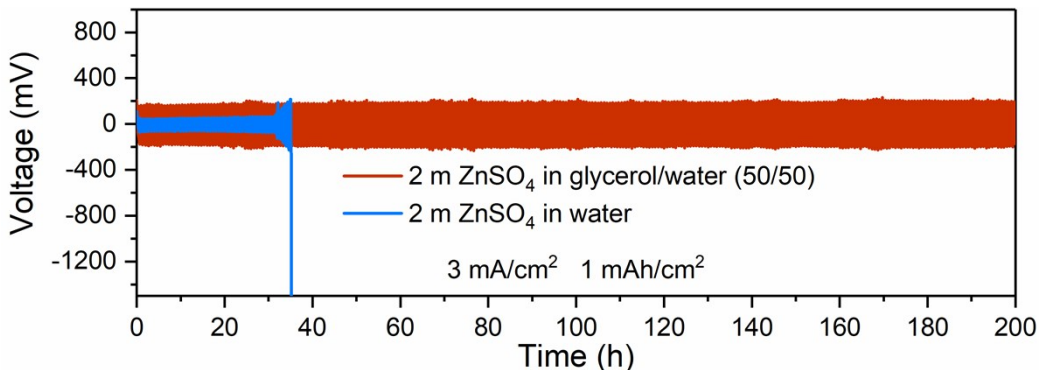

Figure S7. Cycling performance comparison of the symmetric cells in aqueous and hybrid electrolytes at 3 mA cm^{-2}.

Table S1 The performance comparison of symmetric cells for various hybrid electrolyte.

Electrolyte	Current density (mA cm^{-2})	Capacity (mAh cm^{-2})	Voltage hysteresis (mV)	Life (h)	Reference
0.5 M $Zn(CF_3SO_3)_2$ in TEP-H_2O (9:1)	0.25	0.25	~76	~1020	9
0.5 M $Zn(CF_3SO_3)_2$ in TEP-H_2O (8:2)	0.25	0.25	~80	~1020	
0.5 M $Zn(CF_3SO_3)_2$ in TEP-H_2O (7:3)	0.5	0.5	~140	~1020	
2 M $ZnSO_4$/H_2O+50% EG	1	1	~86	1200	10
1 M $Zn(CF_3SO_3)_2$ in (ACN-H_2O) in a volumetric ratio of 3:1	1	1	38	~1300	11
2 M $ZnSO_4$ in EG/water (40/60)	2	1	~50	145	12
3 M $Zn(CF_3SO_3)_2$ with 0.1 M $Mn(CF_3SO_3)_2$ in water with 2 vol% of diethyl ether	0.2	0.2	~25	250	13
1 M $Zn(ClO_4)_2$ in H_2O-EC/EMC(4/6)	2	2	~85	400	14
2 M $ZnSO_4$ in glycerol/water (50/50)	0.2	0.2	73	1500	This work
	0.5	0.5	104	1500	
	1	1	106	1500	
	1	3	59	1000	
	2	2	137	700	
	2	6	61	900	

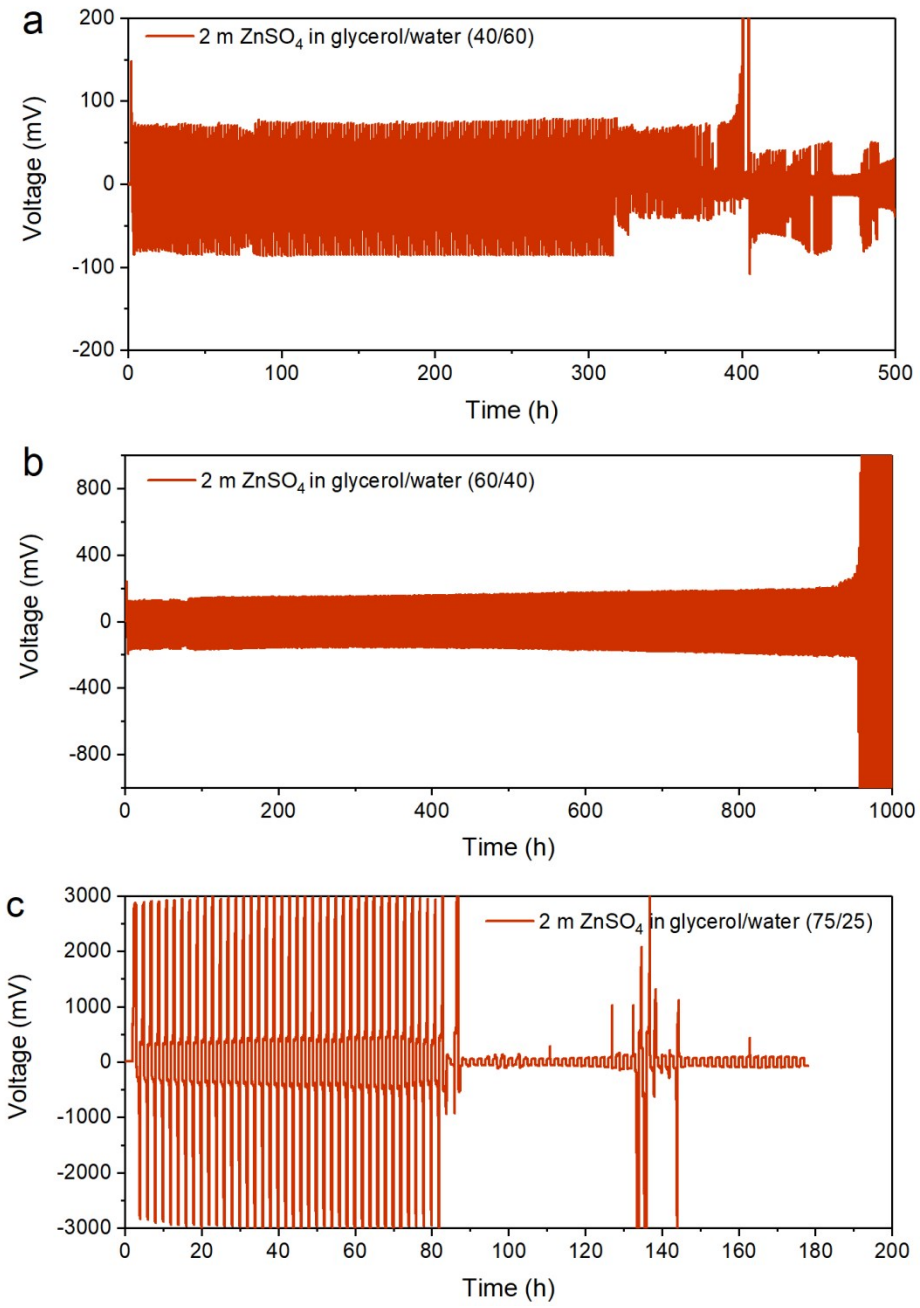

Figure S8. Voltage profiles of the symmetric cells as a function of time at 1 mA cm^{-2} and 1 mAh cm^{-2},

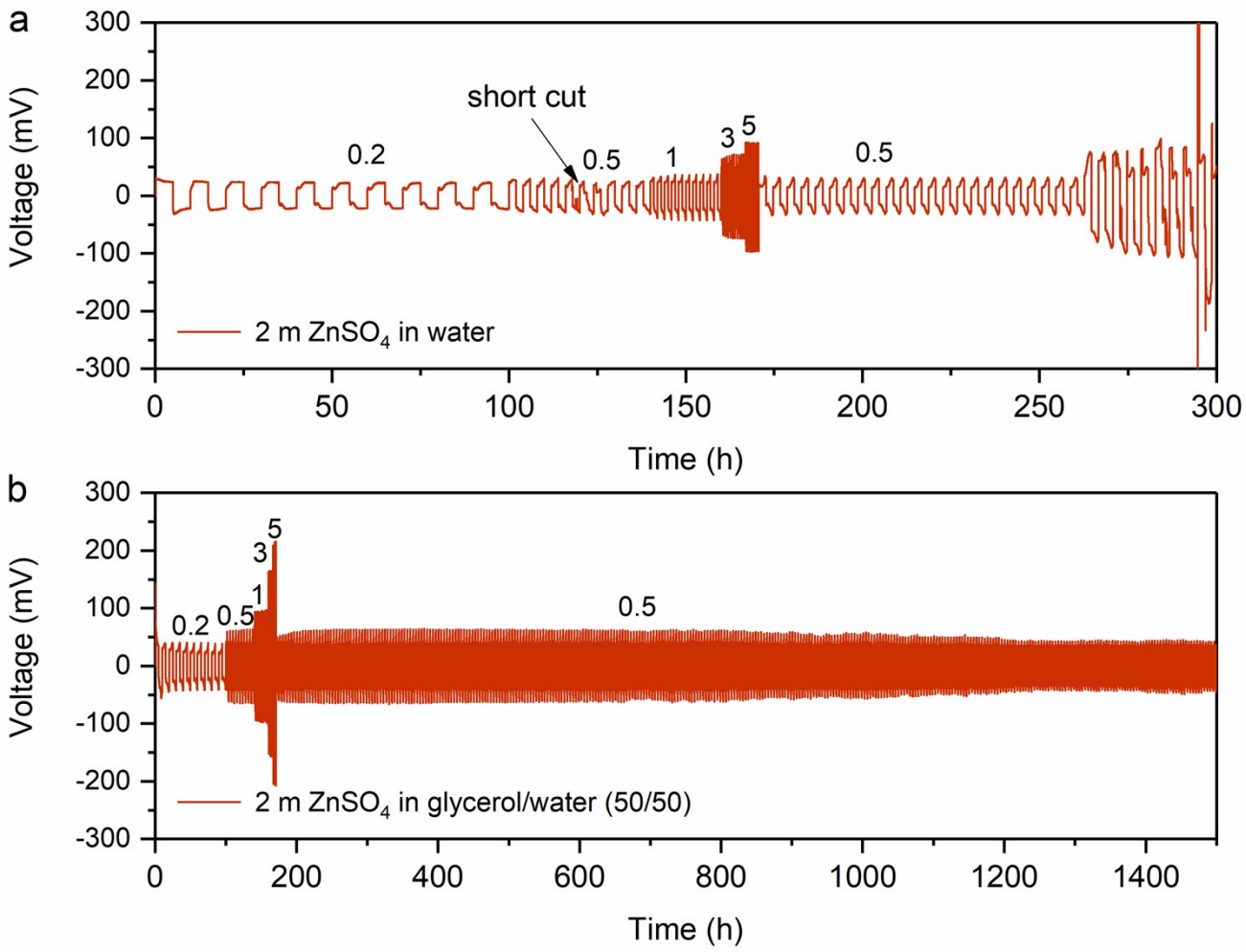

Figure S9. The rate performance of symmetric cells in the aqueous and hybrid electrolytes.

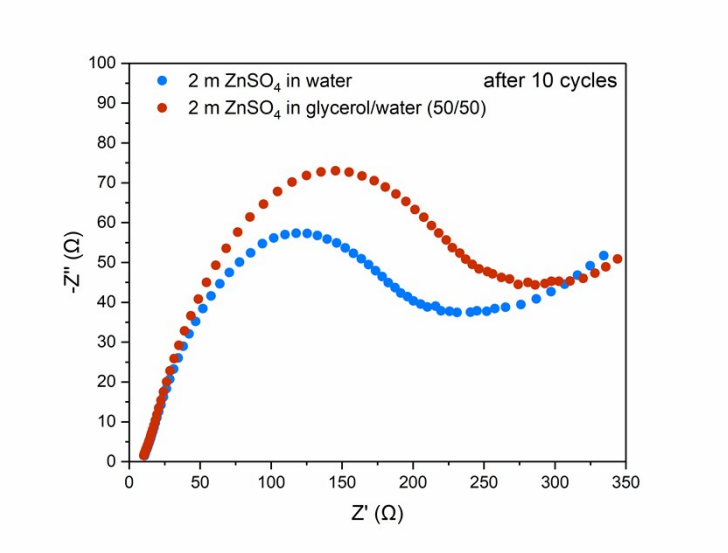

Figure S10. Electrochemical impedance spectra of symmetric Zn||Zn cells in aqueous and hybrid electrolytes.

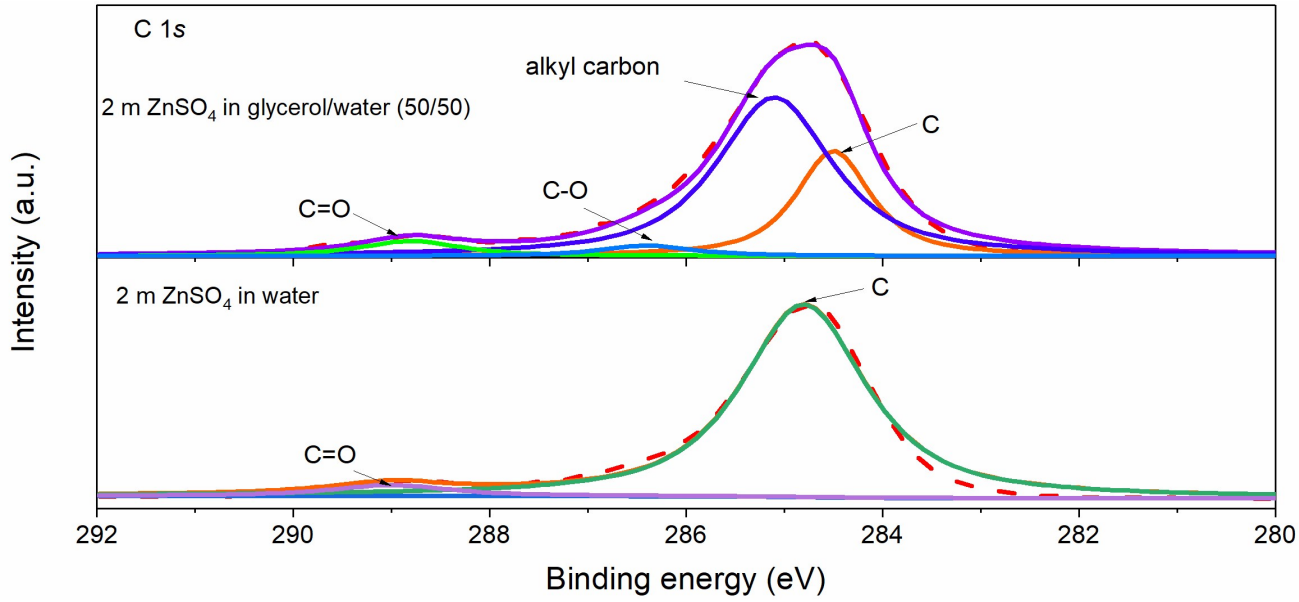

Figure S11. XPS C1s spectrum of the surface of the Zn foil after 10 cycles. Two additional peaks appear after cycle in glycerol/water electrolyte, the species at ~285 eV is ascribed to alkyl carbon and ~286.4 eV is ascribed to C-O species, indicating the presence of glycerol on the surface of cycled Zn.

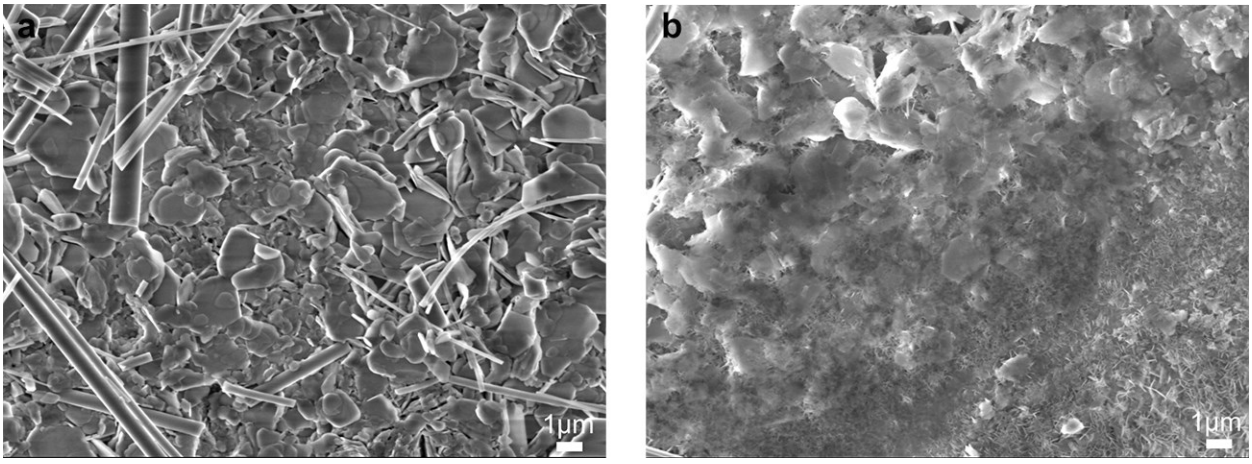

Figure S12. SEM images of the deposited Zn on the SS substrate after plating for 3 mAh cm^{-2} (a) in 2 M $ZnSO_4$ aqueous electrolyte and (b) in 2 M $ZnSO_4$ glycerol/water (50/50) hybrid electrolyte.

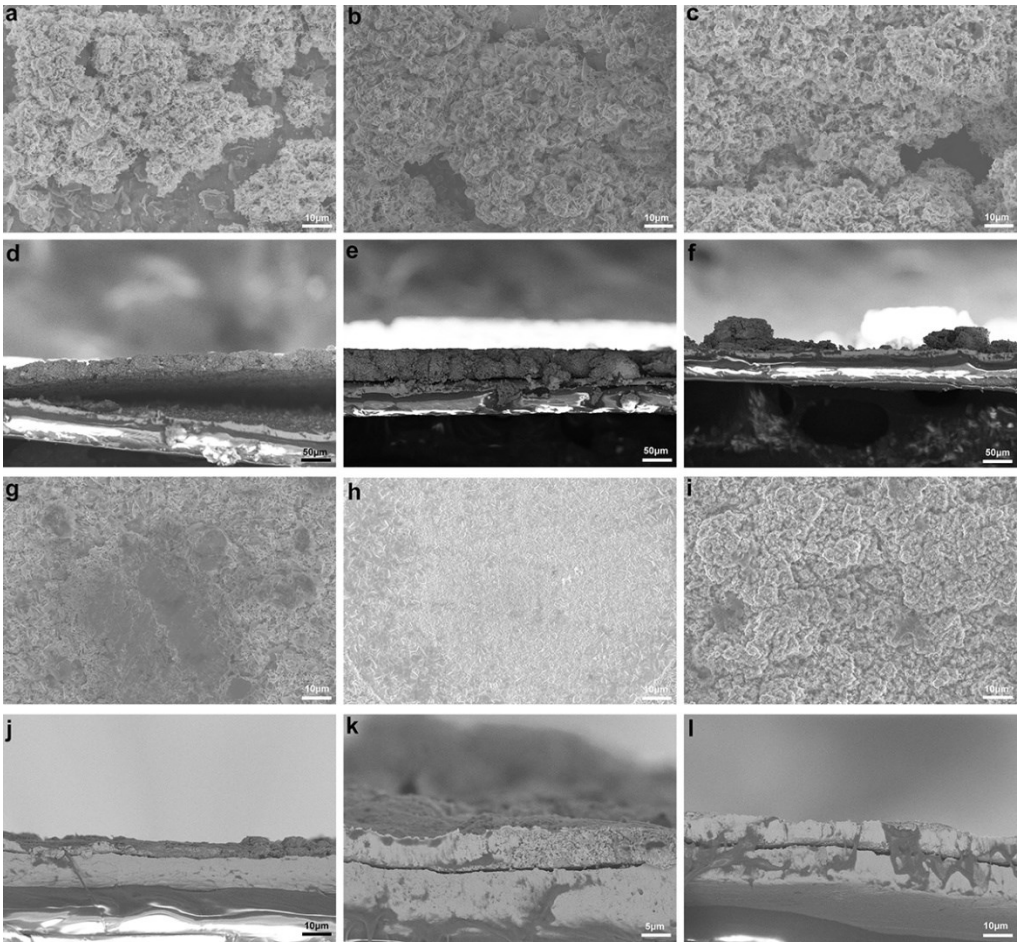

Figure S13. (a-f**)** Top-view and cross-sectional SEM images of the deposited Zn of (a, d) 2 mAh cm^{-2}, (b, e) 4 mAh cm^{-2} and (c, f) 6 mAh cm^{-2}on the SS substrate in 2 M $ZnSO_4$ aqueous electrolyte. Top-view and cross-sectional SEM images of the deposited Zn of (g, j) 2 mAh cm^{-2}, (h, k) 4 mAh cm^{-2} and (i, l) 6 mAh cm^{-2} on the SS substrate in 2 M $ZnSO_4$ glycerol/water (50/50) electrolyte. The deposition current density is 2 mA cm^{-2}. It should be noted that the deposited Zn of 6 mAh cm^{-2} in aqueous electrolyte is very fragile, and only incomplete cross-section was observed in Figure S13f.

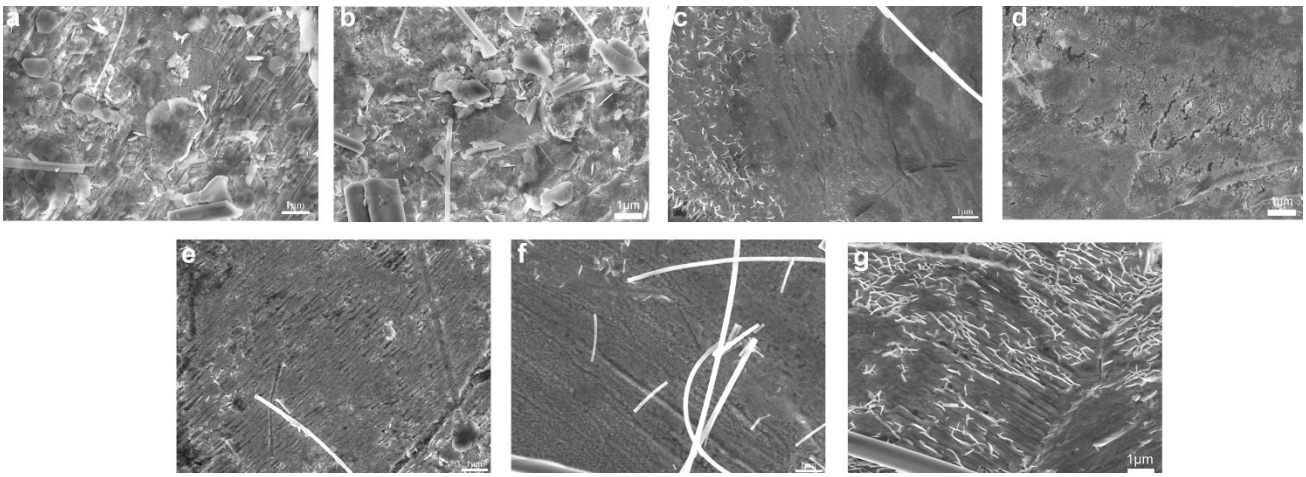

Figure S14. (a-b**)** SEM images of the Zn foil after cycled at 1 mA cm^{-2} for (a) 2 h and (b) 20 h in 2 M $ZnSO_4$ aqueous electrolyte. **(**c-g**)** SEM images of Zn foil after cycled at 1 mA cm^{-2} for (c) 2 h, (d) 20 h, (e) 100 h, (f) 200 h, and (g) 500 h in 2 M $ZnSO_4$ glycerol/water (50/50) electrolyte.

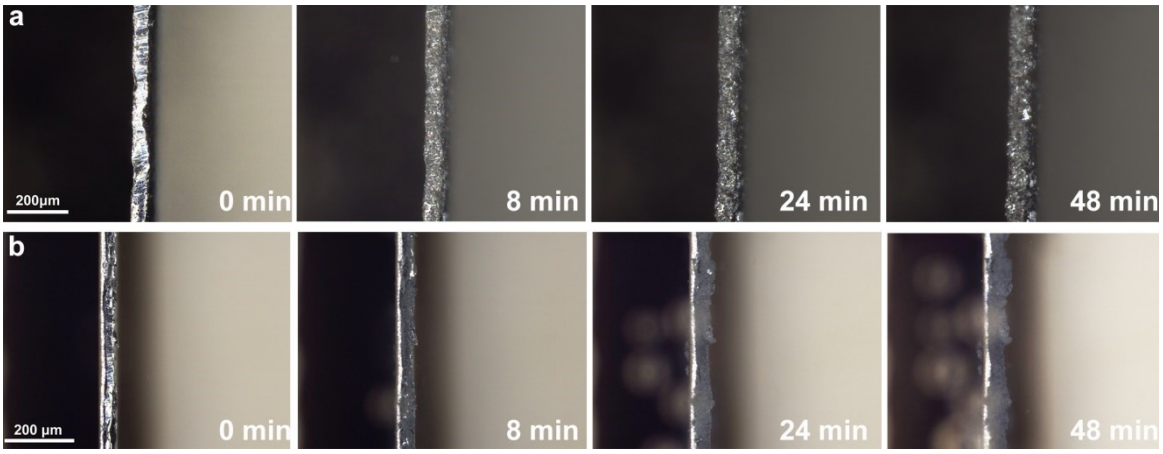

Figure S15. In situ optical microscopy observations of the Zn deposition process at a current density of 3 mA cm^{-2}:(a) in 2 M $ZnSO_4$ aqueous electrolyte and (b) in 2 M $ZnSO_4$ glycerol/water (50/50) electrolyte.

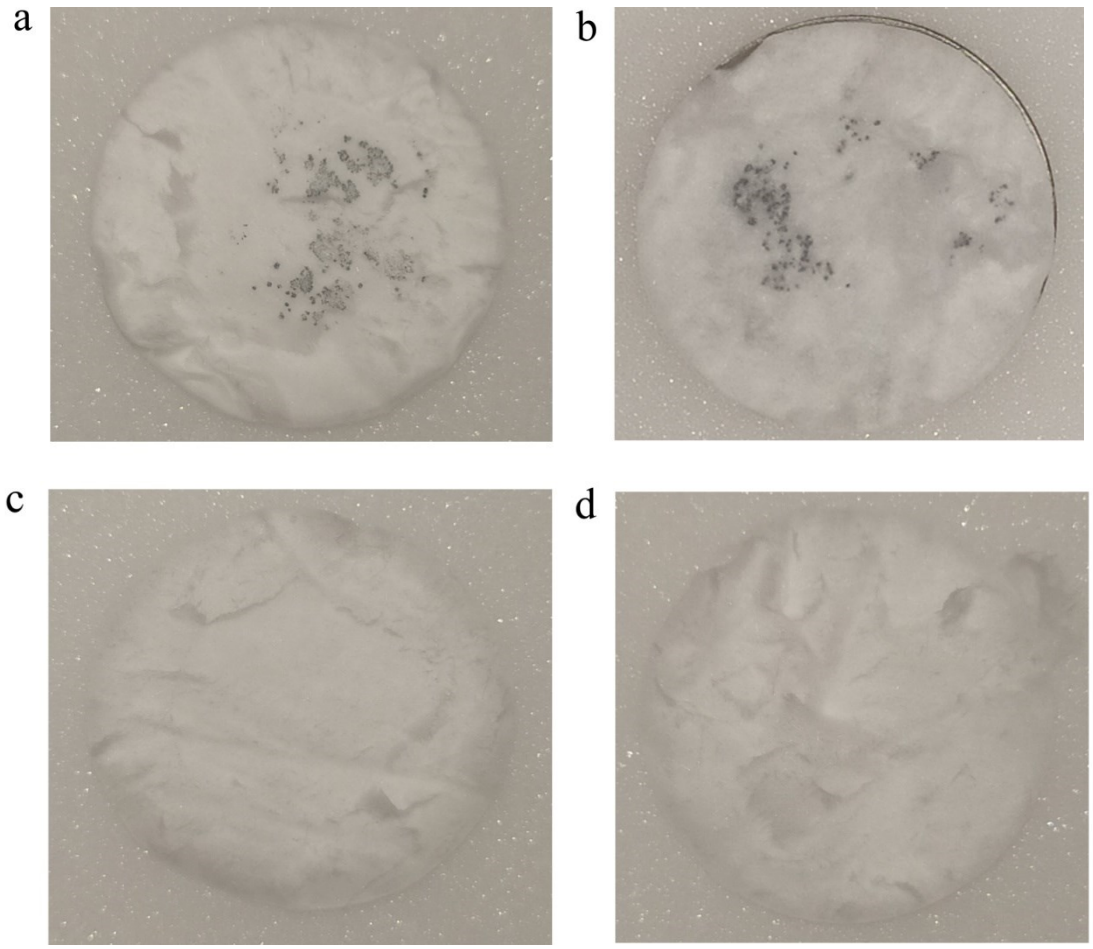

Figure S16. Digital photos of glass fiber separator in symmetric cells using 2 M $ZnSO_4$ aqueous electrolyte after (a) 10 cycles and (b) 20 cycles; using 2 M $ZnSO_4$ glycerol/water (50/50) hybrid electrolyte after (c) 10 cycles and (d) 20 cycles.

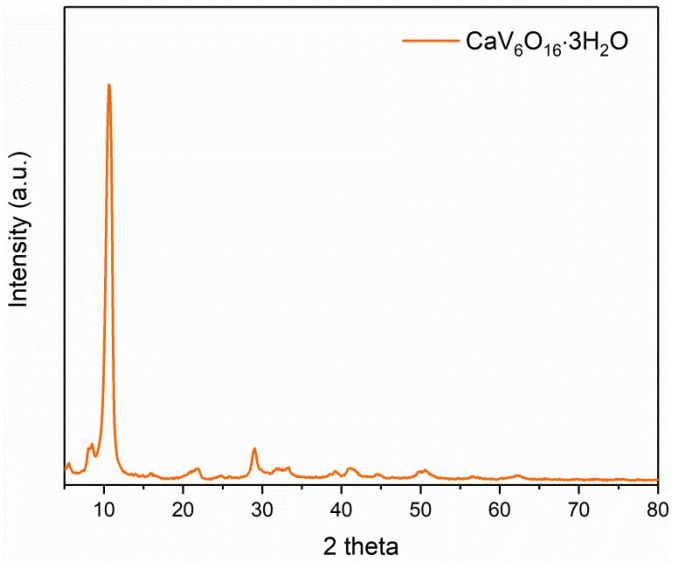

Figure S17. XRD pattern of CaVO powders.

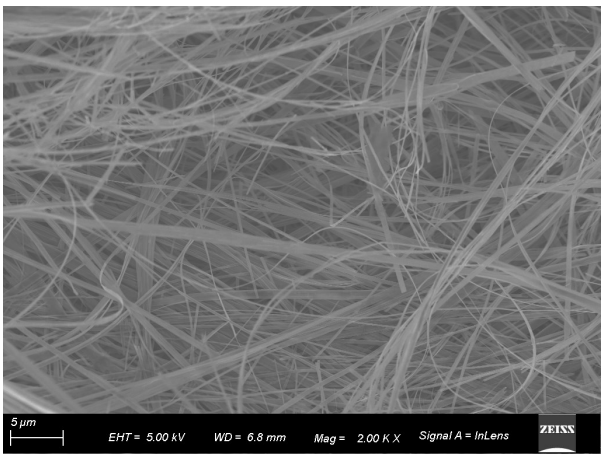

Figure S18. SEM image of the CaVO powders.

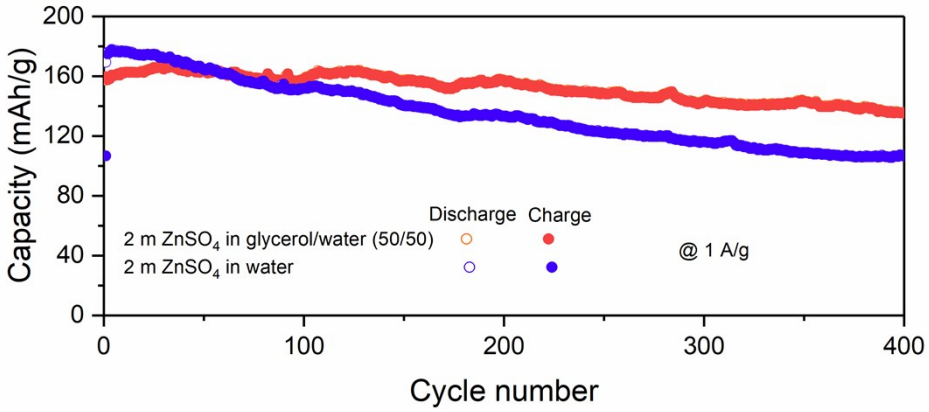

Figure S19. Cycling performance of the Zn||CaVO full cells in aqueous and hybrid electrolytes at 1 A g^{-1}.

References

(1) Y. Zhang, F. Wan, S. Huang, S. Wang, Z. Niu and J. Chen, A chemically self-charging aqueous zinc-ion battery. *Nature communications*, **2020**, 11.

(2) Kohn, W.; Sham, L. J., Self-Consistent Equations Including Exchange and Correlation Effects. *Physical Review* **1965,** *140* (4A), A1133-A1138.

(3) Aleksandr V. Marenich; Christopher J. Cramer; Truhlar, D. G., Universal Solvation Model Based on Solute Electron Density and on a Continuum Model of the Solvent Defined by the Bulk Dielectric Constant and Atomic Surface Tensions. *J. Phys. Chem. B* **2009,** *113* (18), 6378-6369.

(4) M. J. Frisch; G. W. Trucks; H. B. Schlegel; G. E. Scuseria; M. A. Robb; J. R. Cheeseman; G. Scalmani; V. Barone; B. Mennucci; G. A. Petersson; H. Nakatsuji; M. Caricato; X. Li; H. P. Hratchian; A. F. Izmaylov; J. Bloino; G. Zheng; J. L. Sonnenberg; M. Hada; M. Ehara; K. Toyota; R. Fukuda; J. Hasegawa; M. Ishida; T. Nakajima; Y. Honda; O. Kitao; H. Nakai; T. Vreven; J. A. Montgomery; Jr.; J. E. Peralta; F. Ogliaro; M. Bearpark; J. J. Heyd; E. Brothers; K. N. Kudin; V. N. Staroverov; R. Kobayashi; J. Normand; K. Raghavachari; A. Rendell; J. C. Burant; S. S. Iyengar; J. Tomasi; M. Cossi; N. Rega; J. M. Millam; M. Klene; J. E. Knox; J. B. Cross; V. Bakken; C. Adamo; J. Jaramillo; R. Gomperts; R. E. Stratmann; O. Yazyev; A. J. Austin; R. Cammi; C. Pomelli; J. W. Ochterski; R. L. Martin; K. Morokuma; V. G. Zakrzewski; G. A. Voth; P. Salvador; J. J. Dannenberg; S. Dapprich; A. D. Daniels; Ö. Farkas; J. B. Foresman; J. V. Ortiz; J. Cioslowski; D. J. Fox, G09. *Gaussian, Inc., Wallingford CT,* **2009**.

(5) John P. Perdew; Kieron Burke; Ernzerhof, M., Generalized Gradient Approximation Made Simple. *Phys. Rev. Lett.* **1996,** *77* (18), 3865-3868.

(6) H.Sun; P.Ren; J.R.Fried, The COMPASS force field: parameterization and validation for phosphazenes. *Comput. Theor. Polym. Sci.* **1998,** *8* (1-2), 229-246.

(7) George B. Sigal; Milan Mrksich; Whitesides, G. M., Effect of Surface Wettability on the Adsorption of Proteins and Detergents. *J. Am. Chem. Soc.* **1998,** *120* (14), 3464-3473.

(8) Sun, H., COMPASS: An ab Initio Force-Field Optimized for Condensed-Phase ApplicationsOverview with Details on Alkane and Benzene Compounds. *J. Phys. Chem. B* **1998,** *102* (38), 7338-7364.

(9) Naveed, A.; Yang, H.; Yang, J.; Nuli, Y.; Wang, J., Highly reversible and rechargeable safe Zn

batteries based on a triethyl phosphate electrolyte. *Angew. Chem., Int. Ed.* **2019,** *58* (9), 2760-2764.

(10) Wang, N.; Yang, Y.; Qiu, X.; Dong, X.; Wang, Y.; Xia, Y., Stabilized Rechargeable Aqueous Zinc Batteries Using Ethylene Glycol as Water Blocker. *ChemSusChem* **2020**. Doi: 10.1002/cssc.202001750

(11) Shi, J.; Xia, K.; Liu, L.; Liu, C.; Zhang, Q.; Li, L.; Zhou, X.; Liang, J.; Tao, Z., Ultrahigh coulombic efficiency and long-life aqueous Zn anodes enabled by electrolyte additive of acetonitrile. *Electrochimica Acta* **2020,** *358,* 136937.

(12) Chang, N.; Li, T.; Li, R.; Wang, S.; Yin, Y.; Zhang, H.; Li, X., An Aqueous Hybrid Electrolyte for Low-Temperature Zinc-Based Energy Storage Devices. *Energy & Environmental Science* **2020**. Doi: 10.1039/D0EE01538E

(13) Xu, W.; Zhao, K.; Huo, W.; Wang, Y.; Yao, G.; Gu, X.; Cheng, H.; Mai, L.; Hu, C.; Wang, X., Diethyl ether as self-healing electrolyte additive enabled long-life rechargeable aqueous zinc ion batteries. *Nano Energy* **2019,** *62*, 275-281.

(14) Huang, J.-Q.; Guo, X.; Lin, X.; Zhu, Y.; Zhang, B., Hybrid Aqueous/Organic Electrolytes Enable the High-Performance Zn-Ion Batteries. *Research* **2019,** *2019*, 1-10.